Biomechanics and Modeling in Mechanobiology
https://doi.org/10.1007/s10237-024-01919-2

ORIGINAL PAPER

Hyperelastic constitutive modeling of healthy and enzymatically mediated degraded articular cartilage

Asif Istiak[1] · Saiful Islam[1] · Malek Adouni[2] · Tanvir R. Faisal[1]

Received: 3 April 2024 / Accepted: 11 December 2024

Abstract
This research demonstrates a systematic curve fitting approach for acquiring parametric values of hyperelastic constitutive models for both healthy and enzymatically mediated degenerated cartilage to facilitate finite element modeling of cartilage. Several widely used phenomenological hyperelastic constitutive models were tested to adequately capture the changes in cartilage mechanics that vary with the differential/unequal abundance of matrix metalloproteinases (MMPs). Trauma and physiological conditions result in an increased production of collagenases (MMP-1) and gelatinases (MMP-9), which impacts the load-bearing ability of cartilage by significantly deteriorating its extracellular matrix (ECM). The material parameters in the constitutive equation of each hyperelastic model are significant for developing a comprehensive computational interpretation of MMP mediated degenerated cartilage. Stress–strain responses obtained from indentation test were fitted with selected Ogden, polynomial, reduced polynomial, and van der Waals hyperelastic constitutive models by optimizing their adjustable parameters (material constants). The goodness of fit of the 2nd order reduced polynomial and van der Waals model exhibited the closest data fitting with the experimental stress–strain distributions of healthy and degraded articular cartilage. The coefficient of the shear modulus for the 2nd order reduced polynomial decreased gradually by 21.9% to 80.1% with more enzymatic degradation of collagen fibril due to the relative abundance of MMP-1 (collagenases), and 28.5% to 69.2% for the van der Waals model. Our findings showed that the major materials coefficients of the models were reduced in the degenerated cartilages, and the reduction varied differentially with the relative abundance of MMPs-1 and 9, correlating the severity of degeneration. This work advances the understanding of cartilage mechanics and offers insights into the impact of biochemical (enzymatic) effects on cartilage degradation.

Keywords Phenomenological model · Hyperelastic constitutive model · MMP · Enzymatic degradation · Articular cartilage

1 Introduction

Articular cartilage is a thin layer of soft tissue covering the extremities of bones within diarthrodial joints, serving as the contact surface for transferring loads between bones and enabling smooth joint articulation with minimal friction (Ateshian et al. 2005). Changes and alterations in the soft tissues create complex mechanisms that are yet to be fully understood. The degeneration of cartilage due to osteoarthritis (OA) alters its extracellular matrix (ECM) comprising primarily type II collagen fibrils and proteoglycans (PG), leading to changes in its mechanical properties (Mixon et al. 2021; Robinson et al. 2016; Setton et al. 1999). Whilst aggrecan (PG) loss can be reversed, collagen degradation is irreversible, and cartilage cannot be repaired once collagen is largely digested (Karsdal et al. 2008). The ECM degradation is primarily orchestrated by the upregulations of proteases like matrix metalloproteinases (MMPs). Classically, MMPs play a dominant role in the breakdown of the ECM macromolecules and are collectively capable of degrading all ECM components (Grenier et al. 2014). In vitro cartilage degradation is commonly mediated by tumor necrosis factor α (TNFα), interleukin-6 (IL-6) (Sui et al. 2009), IL-1 (Kar et al. 2016a, 2016b), chondroitinase ABC and hyaluronidase (Merrild et al. 2022), bacterial collagenase (Grenier et al.

Asif Istiak and Saiful Islam have contributed equally.

✉ Tanvir R. Faisal
tanvir.faisal@louisiana.edu

[1] Department of Mechanical Engineering, University of Louisiana at Lafayette, Lafayette, LA 70503, USA

[2] Abdullah Al Salem University, Biomedical and Instrumentation Engineering, Khalidiya, Kuwait

Published online: 19 January 2025

2014), Collagenase type VII and trypsin (Saarakkala et al. 2004; Töyräs et al. 1999; Wang et al. 2008) to stimulate OA, but the collective effect of metalloproteinases on the biomechanical properties of cartilage tissue has been scarcely or not systematically studied.

In the progression of OA, the early and potentially reversible depletion of PG is initiated by aggrecanases such as a disintegrin and metalloproteinase with thrombospondin motifs (ADAMTSs) as well as MMPs in articular cartilage (Galloway et al. 1983; Karsdal et al. 2008). Collagenases, MMP-1 and MMP-13, have predominant roles in OA; generally, the cleavage of collagen type II occurs in the pericellular and superficial sites of the articular cartilage, where both MMPs-1 and 13 are localized (Fernandes et al. 1998; Moldovan et al. 1997; Xia et al. 2002). Expression of other MMPs such as MMPs-2, 9, and 3, is also elevated in arthritis, and these enzymes degrade non-collagen matrix components of the joints (Burrage et al. 2006). MMP-1 begins the process of collagen degradation, while MMP-9 further breaks down the resulting collagen fragments creating a cascade effect that more accurately reflects the intricate process of cartilage destruction in OA (Mixon 2021; Mixon et al. 2021, 2022). Once the collagen triple helix is cleaved by the collagenases (MMP-1), the denatured collagens that turns into gelatins along with proteoglycan core protein–aggrecan are digested by MMP-9 (gelatinases), which is elevated in moderate to severe OA patients and contributes to the cartilage ECM loss (Smith Jr 2006). Given these considerations, this study focused on assessing the mechanics of cartilage degradation with a combination of collagenases (MMP-1) and gelatinases (MMP-9), which are responsible for breaking down collagen fibrils, and thereby compromising the bulk mechanical properties of cartilage tissue.

Soft biological tissues such as cartilage, ligaments and tendons, polymers, and gels exhibit nonlinear elasticity (Sasson et al. 2012; Shearer 2015). Although several nonlinear approaches such as hyperelastic (Brown et al. 2009; Henak et al. 2014; Robinson et al. 2016), viscoelastic (Ma and Arruda 2013; Richard et al. 2013), and poroelastic (Tan et al. 2023) models have been employed to portray mechanical properties of control cartilage, we primarily utilized hyperelastic models in this study to capture the effect of enzymatic degradation in cartilage. The hyperelastic models are widely used in soft tissues that undergo large deformation (Mansouri and Darijani 2014; Tan et al. 2023) due to their computational efficiency and proven accuracy in predicting the transient mechanical behavior during the cartilage loading phase. In comparison with viscoelastic and poroelastic models, hyperelastic models are computationally less expensive, because they do not account for time-dependent behavior or fluid flow, allowing for faster simulations with fewer parameters to solve (Klets et al. 2016; Weizel et al. 2022). Hyperelasticity is commonly studied using a phenomenological approach when the material's stress–strain behavior can be accurately described by hyperelastic constitutive models. Phenomenological models have been formulated based on macroscopic experimental observations, aiming to depict the elastic behavior of these materials. Hence, in this study, we primarily tested different phenomenological models such as neo-Hookean (Treloar 1975), Yeoh (Yeoh 1993), Ogden (Ogden 1972), Mooney-Rivlin (Mooney 1940; Rivlin 1948), polynomial (Rivlin and Saunders 1951), van der Waals (Kilian et al. 1986), and reduced polynomial (Lin et al. 2023) models. The material parameters of phenomenological models can be obtained by fitting the model equation to the experimental data of a wide variety of materials without understanding the material's microstructural details. These material models, characterized by several adjustable parameters, are fundamentally derived from a strain energy density function (W) that considers energetic path relationships, correlating the strain energy of a material with the deformation gradient. The strain energy based phenomenological approach has been often utilized to characterize biological tissues and elastomers (Karimi et al. 2017; Previati et al. 2017) as it is computationally efficient.

Hyperelastic constitutive modeling is suitable for cartilage tissue because the strain energy density function not only captures the nonlinear stress–strain relationship but also accounts for its incompressible behavior (Henak et al. 2014). However, there is limitation of comprehensive data on the hyperelastic properties of healthy human cartilage (Anderson et al. 2008; Henak et al. 2014; Khaniki et al. 2023; Pierce et al. 2009; Weizel et al. 2022), and only a few models exist for determining the material constants of degenerated cartilage (Nissinen et al. 2021; Robinson et al. 2016). Prior research demonstrated a correlation between the material constants and tissue composition (Kiviranta et al. 2006; Rieppo et al. 2003) and OA severity (Armstrong and Mow 1982; Kleemann et al. 2005; Saarakkala et al. 2003). Although the material constants in hyperelastic cartilage models are likely to alter due to OA, the magnitude of these changes and whether they can be anticipated based on variations in tissue structure or the severity of OA are currently unknown.

This study focused on the computational simulation of healthy and MMP degraded cartilage based on fitting incompressible hyperelastic constitutive laws to stress–strain experimental data. We hypothesized that the extent of cartilage degeneration due to the differential/unequal abundance of MMP-1 (collagenases) and MMP-9 (gelatinases) that is reflected in cartilage's mechanical integrity will influence the hyperelastic material constants accordingly. Hence, the experimental stress–strain responses of healthy and MMPs mediated degenerated cartilages were fitted with several hyperelastic constitutive models, optimizing the adjustable parameters (material constants) for selected Ogden,

polynomial, reduced polynomial, and van der Waals models. Afterward, finite element analysis (FEA) was conducted using the calibrated material constants. Therefore, the aims of the present study were to 1) determine the hyperelastic material constants of healthy and degraded bovine knee cartilage using isotropic hyperelastic models, and 2) determine correlation, if there is any, between the hyperelastic material constants and cartilage degeneration.

2 Materials and methods

2.1 Experiment

2.1.1 Sample preparation

Articular cartilage plugs attached to subchondral bone were extracted from the stifle joints of mature cows (between 18 and 24 months old) sourced from a local slaughterhouse. The joints were preserved frozen at −80 °C until sample extraction from the medial and lateral femoral condyles utilizing a mosaicplasty tabular chisel (Smith & Nephew 7,209,234) at ambient conditions. A total of 30 articular cartilage explants were harvested from 6 knees of 3 cows, each with a diameter of 3.5 mm and thickness of 5 mm with subchondral bone attached. Throughout the extraction process, phosphate-buffered saline (PBS) was used to moisten the articular surface, safeguarding the cartilage from drying out. Cartilages showing any surface defects or fissures upon visible inspection were carefully excluded during the extraction. The collected samples were preserved at −20 °C enveloped in PBS-moistened gauze until required for testing. To mitigate the effects of freeze–thaw cycles, all samples underwent single thaw cycle (Changoor et al. 2010) even though prior studies indicated that freeze–thaw cycles had minimal impact on the mechanical properties of articular cartilage explants (Athanasiou et al. 1994; Szarko et al. 2010).

Before testing, the thickness of each sample, excluding the subchondral bone, was measured using a needle probe at the four corners of the plug with the Mach-1 v500c micromechanical tester (Biomomentum Inc.). The mean thickness of the cartilage was determined to be 1.30 ± 0.08 mm (Fig. 1).

2.1.2 Sample degradation

To simulate *in vivo* conditions, we prepared a 2% agarose gel using solid agar (Sigma–Aldrich) and TAE buffer (Sigma–Aldrich), carefully pipetting it around each sample until only the top of the articular surface remained exposed to the enzyme solution (Mixon et al. 2021, 2022). To induce downward degradation from the articular surface, each explant was individually placed in the wells of a standard Corning cell culture well plate (Sigma–Aldrich). The preparation of MMPs followed a careful protocol to ensure optimal enzyme activity. Initially, the vials containing lyophilized MMP powder were gently tapped to consolidate the contents at the bottom before opening. Following the manufacturer's (BioVision) guidelines, the MMPs were reconstituted in PBS solution to achieve a concentration of 0.5 mg/ml and left to stabilize for 30 min. During the reconstitution process, the vials were gently agitated to facilitate dissolution, avoiding vigorous shaking that could lead to foaming and protein denaturation. After preparing the appropriate dilutions, 200 µL aliquots were stored at −20 °C for future use in enzymatic degradation experiments. To simulate the natural progression of cartilage degradation, individual explants were placed in separate wells, allowing for controlled exposure to the enzyme solution from the articular surface downward. With closed lid, the enzymatically treated samples were incubated at 5% CO_2 for 44 hrs in a 37 °C incubated environment in the standard well plate. The samples were agitated gently every 12 hrs for a good diffusion. The digestion solution was rinsed away with PBS solution before the testing and soaked into PBS solution during the testing. After the incubation, all the samples were tested within 2 days, each sample was tested again after 2 hrs of the first test to allow recover cartilage's structural integrity (Korhonen et al. 2002). The agarose gel was allowed

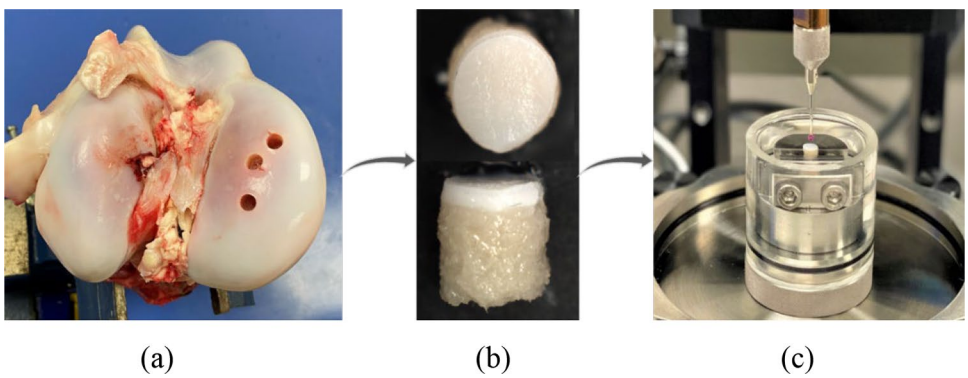

Fig. 1 **a** Sample extracted from femoral condyles, **b** Extracted cartilage explant with subchondral bone, and **c** Indentation testing of cartilage samples in Mach-1 v500c mechanical tester

to cool and solidify for 30 min; after that, the activated human recombinant MMP-1 and MMP-9 (BioVision, Milpitas, CA) were loaded onto the articular top surface at varying concentrations. These enzymes were applied to each group of sample size 10, as outlined in Table 1. The concentration scale of MMPs was chosen based on earlier studies concerning the pro-form of enzyme detection in synovial fluid from arthritis patients using immunoassays (ELISA) (Tchetverikov et al. 2005).

2.1.3 Indentation testing

Indentation has been a widely used testing method for assessing the mechanical properties of soft tissues such as articular cartilage (Chen et al. 2004; Korhonen et al. 2002; Lyyra et al. 1999; Mixon 2021) and was adopted in this study to characterize the structural integrity of the cartilage. Each cartilage sample was placed in an osteochondral core holder and submerged in a PBS bath to avert desiccation of the articular surface after removal from the MMP cocktail and agarose. Indentation was conducted using a spherical indenter (1 mm dia.) via the Mach-1 v500c (Biomomentum Inc.) testing apparatus (Bae et al. 2006, 2007). The spherical indenter was used to reduce cartilage damage and apply more centralized compression than the pyramid and other sharp indenters. Each sample was compressed at a strain rate of 0.1%/sec until the total strain reached 20%, falling within the elastic limit and mimicking a typical physiological loading condition (Park et al. 2004). The considered slow strain rate represents controlled cartilage loading rate that allows stress dissipation by fluid flow throughout whole loading time (Henak et al. 2014; Kabir et al. 2021). All samples, before and after enzymatic treatment, were subjected to indentation tests to compare the changes in their mechanical properties. Different factors, such as age (Lotz and Loeser 2012), sex (Hernandez et al. 2022), and the specific characteristics of the site (Linus et al. 2024) from where the cartilages are extracted may contribute to the variations in cartilage mechanics. Therefore, to exclude the effect of these variabilities in each degradation model, distinct control baselines were established for each type of degradation (Mixon et al. 2021, 2022).

Table 1 Concentration ratios of MMP-1 (collagenases) and MMP-9 (gelatinases) used to degrade articular cartilage samples

MMP-1 (c) concentration (ng/ml)	MMP-9 (g) concentration (ng/ml)	c:g ratio
4	4	1:1
2	6	1:3
6	2	3:1

2.2 Hyperelastic materials modeling

The combination of hyperelastic constitutive modeling and FEA enables accurate prediction of mechanical properties in both healthy and degraded cartilage under indentation loading. FEA serves as a valuable assessment tool for investigating the impact of biochemical alterations caused by degradative enzymes and biomechanical loading on cartilage, allowing researchers to quantify the stress and strain experienced by both healthy and compromised tissue during loading scenarios. This FE simulation approach is versatile and can be extended to analyze other soft tissues and biopolymers with more intricate geometries and complex loading conditions.

2.2.1 Kinematics of finite deformations

To simulate the hyperelastic behavior of cartilage, the principles of nonlinear continuum mechanics were applied. This theory describes the physical phenomena of the system at a continuum level without explicitly taking into account the intricate microstructure. The continuum body $B_o \in \mathbb{R}^3$ comprises continuum points $P \in B_o$ and exhibits a continuous and homogeneous distribution of matter in both space and time. The dimensions of a continuum body are greater than those of the microstructures within the body. The kinematics of finite deformation of the undeformed body $B_o \in \mathbb{R}^3$ at time $t = 0$ can be explained through the deformation maps $\boldsymbol{\varphi}$ that map the position $\mathbf{X}$ in the reference or material configuration B_o at the initial position to its new position $\mathbf{x} = \boldsymbol{\varphi}(\mathbf{X}, t)$ in the deformed, current, or spatial configuration B_t. The deformation gradient to map undeformed configurations to deformed configurations is defined as $F(X,t) = \nabla_{X\varphi}(X,t)$ (Gasser and Holzapfel 2002). For a uniaxial deformation characterized by compression and tension, where the material is incompressible and homogeneous, the deformation gradient is expressed as follows:

$$F = \begin{bmatrix} \lambda_1 & & \\ & \lambda_2 & \\ & & \lambda_3 \end{bmatrix} \text{ with } \lambda_1 = \lambda \; \lambda_{2,3} = 1\Big/\sqrt{\lambda}.$$

where λ_1, λ_2, and λ_3 are the principal stretches along the principal direction and λ is the axial stretch. $\lambda_{1\to3}$ are the square roots of the eigenvalues of the right Cauchy–Green deformation tensor C defined as $C = F^T F$, whose invariants are I_1, I_2, and I_3 such that

$$I_1 = \lambda_1^2 + \lambda_2^2 + \lambda_3^2$$
$$I_2 = \lambda_1^2\lambda_2^2 + \lambda_2^2\lambda_3^2 + \lambda_3^2\lambda_1^2 \quad (1)$$
$$I_3 = \lambda_1\lambda_2\lambda_3$$

The cartilage has been assumed to be isotropic and nearly incompressible for the purpose of this study such that the third invariant I_3 equals to one (Moerman et al. 2020; Pelliciari and Tarantino 2020; Steck et al. 2019).

2.2.2 Isotropic hyperelastic material models

Articular cartilage typically undergoes large deformation under compressive (Oloyede and Broom 1996) as well as tensile loading (Woo et al. 1976). In the context of cartilage, we focused on the large-strain and nonlinear time-independent material response, often referred to as finite hyperelastic response, neglecting viscous and porous effects. The constitutive law governing the hyperelastic material relates the strain energy density function W and the deformation gradient, F, the invariants I_1, I_2, and I_3 or the principal stretches λ_1, λ_2, and λ_3 (Holzapfel 2002). A stress measure suitable for analyzing experimental data is nominal stress, calculated as the force divided by the undeformed area of the continuum body. This is also known as the first Piola–Kirchoff stress tensor and is defined as

$$P = J F^{-1}\sigma \quad (2)$$

where σ is the Cauchy stress tensor. The cartilage is assumed to exhibit incompressible material behavior such as $J = \det(F) = 1$. The assumption of incompressibility simplifies the model equations without compromising accuracy.

2.2.3 Hyperelastic material models calibration

In this study, we finally selected four hyperelastic materials models (1st order Ogden, 3rd order polynomial, second order reduced polynomial and van der Waals) to represent the deformation behavior of healthy and degraded cartilage tissues after testing a number of hyperelastic material models. Other models such as Mooney–Rivlin, neo–Hookean, Arruda–Boyce, Yeoh, Ogden (2nd and 3rd order), polynomial (1st and 2nd order), and reduced polynomial (1st and 3rd order) were initially considered. However, they were excluded from further consideration, because they either failed to adequately fit the experimental data or displayed instability. All the calibrations for the hyperelastic data fitting were conducted using MCalibration 7.0 software (Veryst Engineering, Needham, Massachusetts, USA). During the calibration (optimization) process, the objective was to minimize the mean square difference (MSD) between the experimental stress and the stress obtained via the calibrated hyperelastic models (Fig. 2). The calibration process involved an extensive search for optimal parameters to minimize the fitness function. Among various definitions of fitness function (Fernández et al. 2018; López-Campos et al. 2019), we used the mean squared difference, which minimizes the square of the difference between the experimental

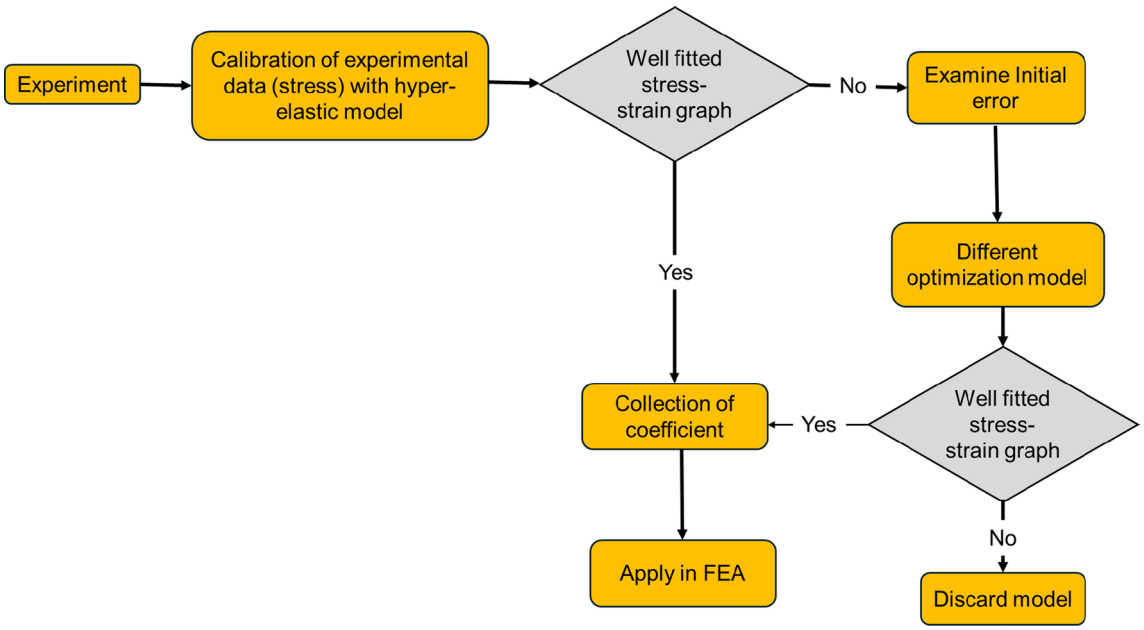

Fig. 2 Workflow of the hyperelastic material model calibration process

stress data and the stress predicted by the hyperelastic material model. In hyperelastic material modeling, the fitness function evaluates how accurately the strain energy function (with its specific parameters) reproduces the stress–strain behavior observed in experiments. A lower value of the fitness function indicates a better fit of the model to the experimental data.

This included an initial random search followed by the application of Levenberg–Marquardt and Nelder–Mead simplex methods. As an optimization technique, Levenberg–Marquardt combines the features of gradient descent and Gauss–Newton methods to solve nonlinear least squares problems (Gavin 2019; Liggett and Chen 1994). The algorithm iteratively adjusts the model parameters to minimize the sum of the squared differences between the predicted and observed stress values. For a specific model, material parameters are initially identified using genetic algorithms, and later the material parameters obtained with this method are used as initial guess of the classical Levenberg–Marquardt method (Levenberg 1944; Marquardt 1963). If this method fails to converge, the mean square method is subsequently applied (Marckmann and Verron 2006).

The simplex Nelder–Mead methods is numerical optimization technique used to find the minimum or maximum of functions in multidimensional spaces (Luersen et al. 2004). This algorithm works systematically moving and reshaping this simplex to find the optimal set of parameters. This method is particularly suitable for this purpose since it minimizes the objective functions during the parameter identification of hyperelastic models (Lagarias et al. 1998). These optimization methods were used to find the optimal set of parameters that best represent the actual material properties observed in experiments with the hyperelastic models.

2.3 Ogden model

The Ogden hyperelastic model, which has been applied to different materials including rubber, polymers, and biological tissues (Budday et al. 2020; Ogden 1972), is a phenomenological model that utilize the strain energy potential (W) that is defined by the principal stretches as follows,

$$W = \sum_{i=1}^{N} \frac{2\mu_i}{\alpha_i^2}\left(\overline{\lambda}_1^{\alpha_i} + \overline{\lambda}_2^{\alpha_i} + \overline{\lambda}_3^{\alpha_i} - 3\right) + \sum_{i=1}^{N} \frac{1}{D_i}\left(J_{el} - 1\right)^{2i}, \quad (3)$$

where $\overline{\lambda}_i$ is the deviatoric principal stretches, $\overline{\lambda}_i = J^{-\frac{1}{3}}\lambda_i$, λ_1, λ_2, λ_3 are the principal stretches; J is the total volume ratio, J_{el} is the elastic volume ratio, N is the order of material parameters, and μ_i, α_i, and D_i are temperature dependent material parameters. In this work, $N \leq 2$ was selected for biomechanical relevance and modeling suitability for biological soft tissues (Budday et al. 2017; Lohr et al. 2022).

In the application of the 1st order Ogden model, a constraint was incorporated such that $u_i\alpha_i\big|_{i=1} > 0$. Material behavior was presumed incompressible, leading to the exclusion of D_i from the optimization process. Consequently, μ_i and α_i are the material parameters optimized during the curve fitting process. Negligible compressibility, quantified as $1e^{-2}$, was allocated to D_i during FEA with all the selected models.

2.4 Polynomial model

The polynomial strain energy density function is presented as follows:

$$W = \sum_{i+j=1}^{N} C_{ij}\left(\bar{I}_1 - 3\right)^i\left(\bar{I}_2 - 3\right)^j + \sum_{i=l}^{N} \frac{1}{D_i}\left(J_{el} - 1\right)^{2i} \quad (4)$$

where I_1 and I_2 represent the first and second strain invariants of the Cauchy–Green strain tensor, C_{ij} and D_i are the material parameters that exhibit temperature-dependence. J_{el} and D_i represent the same as in Eq. (3). While the parameter N can attain values as high as six, values of N exceeding two typically rare when both strain invariants are incorporated. In this study, we assessed 3rd order polynomial strain energy density function and resulted in nine hyperelastic parameters. Distinct variations of the polynomial model can be generated by setting specific coefficients to zero. For instance, when C_{ij} with $j \neq 0$ are set to zero, we get the reduced polynomial form.

2.5 Reduced polynomial model

The expression of reduced polynomial model, derived form of Eq. (4), is as follows,

$$W = \sum_{i=1}^{N} C_{i0}\left(\bar{I}_1 - 3\right)^i + \sum_{i=l}^{N} \frac{1}{D_i}\left(J_{el} - 1\right)^{2i} \quad (5)$$

A 2nd order reduced polynomial strain energy density function was examined in this study, with four hyperelastic parameters. Evidently, this model does not consider the second strain invariants. It is generally recommended to utilize hyperelastic models that are independent of the second invariant when calibration is possible through only a single type of experiment (Bidhendi et al. 2020; Kaliske and Rothert 1997; Yeoh 1993). Based on the satisfactory alignment of this model with our experimental data, this hyperelastic model was considered.

2.6 Van der Waals model

The formula for the van der Waals, also known as the Kilian model (Kilian 1981) strain energy equation is,

$$W = \mu\left\{-\left(\lambda_m^2 - 3\right)[\ln(1-\eta)+\eta] - \frac{2}{3}a\left(\frac{\widetilde{I}-3}{2}\right)^{\frac{3}{2}}\right\} + \frac{1}{D}\left(\frac{J_{el}^2-1}{2} - \ln J_{el}\right), \tag{6}$$

where λ_m is the locking stretch, μ is the initial shear modulus, a is the global interaction parameter, and D controls compressibility. Here, $\tilde{I}$ and η could be defined as

$$\widetilde{I} = (1-\beta)\bar{I}_1 + \beta\bar{I}_2 \tag{7}$$

and

$$\eta = \sqrt{\frac{\widetilde{I}-3}{\lambda_m^2 - 3}}, \tag{8}$$

where β is the invariant mixture parameter. For $\beta = 0.0$, the van der Waals potential will be dependent on the first invariant only.

2.6.1 Goodness of fit

Stress was calculated from the strain energy density functions W of the models considered herein. An objective function is defined to measure the difference between experimental stress and the model predictions. The goodness of fit was used here to present the error.

The goodness of fit was evaluated by the coefficient of determination $\left(R^2\right)$ as follows.

$$R^2 = 1 - \frac{SSR}{SST} \tag{9}$$

where SSR is the sum of squares of the residual, SST represents the total sum of squares.

$$SSR = \sum_{i=1}^{n}\left(y_i - \breve{y}_i\right)^2 \tag{10}$$

$$SST = \sum_{i=1}^{n}\left(y_i - \bar{y}_i\right)^2 \tag{11}$$

where y is the measured value, $\breve{y}$ is the fitted function, and $\bar{y}$ is the mean value of the measured data. The coefficient of determination $\left(R^2\right)$ ranges from 0 to 1, where 1 represents that the fitted parameters perfectly capture experimental data and lower values suggest poorer fit with the experimental data.

2.7 Finite element analysis

FE modeling was conducted in Abaqus 6.14 (Dassault Systèmes) to simulate the experimental indentation tests to capture the nonlinear stress–strain responses of both healthy and degraded cartilages. To accommodate this, we implemented the material constants of the hyperelastic models considered herein.

2.7.1 FE modeling of indentation test

To simulate the indentation test, a cylindrical sample of cartilage (3 mm in diameter and 1.375 mm in thickness) was modeled along with a rigid spherical indenter of 1 mm in diameter. The model was meshed with C3D8H element—Abaqus 3D continuum element with 8-node linear brick, hybrid with constant pressure. This element is particularly suitable for modeling nearly incompressible materials like cartilage (Jaramillo et al. 2015; Suchocki 2017). This hybrid element helps prevent volumetric locking in incompressible materials. The discretization in the cartilage sample was designed to have a finer mesh of 0.025 mm around the sphere while the remaining were coarse mesh of 0.25 mm towards the model's boundaries. (Fig. 3). A mesh convergence was performed to achieve mesh independence on the computation of the field variables and the global response of the cartilage.

Similar to the experiment, the model's base was completely fixed, and frictionless contact was modeled between the indenter ball and the articular cartilage surface. Quasi-static finite element simulations were executed in the Abaqus/Standard solver. The model parameters included an indentation of 0.275 mm over a 200 sec timeframe, simulating a physiological strain of 20% at a strain rate of 0.1%/sec. The parameters for the hyperelastic models were determined

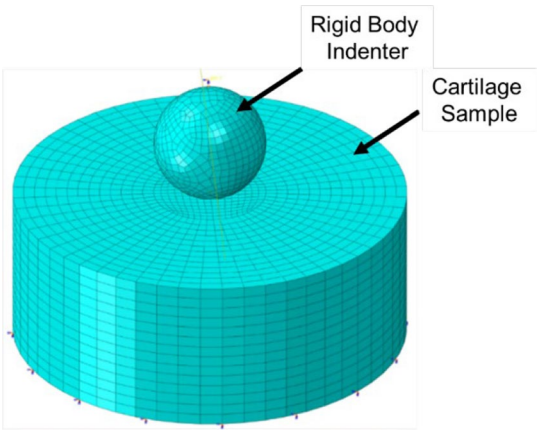

Fig. 3 Finite element meshed model of cartilage with rigid ball indenter and fixed boundary conditions at the bottom. The indenter ball is aligned with the center of the cartilage model

from the initial curve fitting, as mentioned in Sect. 2.2, and incorporated into the hyperelastic constitutive models to conduct FEA.

3 Results

All the specimens, irrespective of healthy or degraded groups, were subjected to a bulk strain of 20% in accordance with the physiological strain limit (Bingham et al. 2008; Carter et al. 2015; Coleman et al. 2013; Patel et al. 2019; Sutter et al. 2015). Figure 4 shows the experimental stress–strain plots along with the fitted hyperplastic material models for both healthy (Fig. 4a) and degraded cartilages (Figs. 4b–d). It is evident that all the hyperelastic models fit well within the upper and lower bounds of the experiments irrespective of whether the cartilage was healthy or degraded. However, in comparison with the mean value of the experiments, the 1st order Ogden, 3rd order polynomial, and 2nd order reduced polynomial

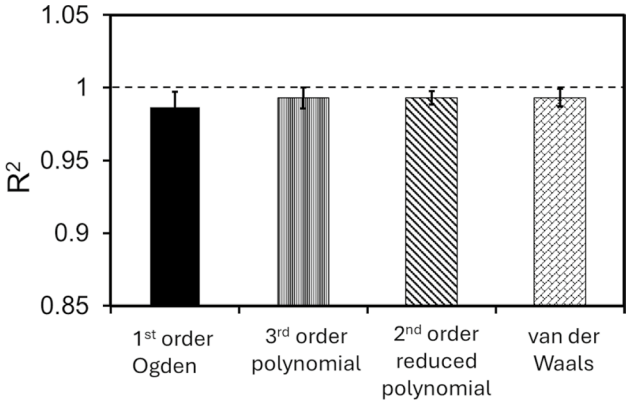

Fig. 5 Comparison of coefficient of determination (R^2) (mean ± *SD*) of healthy and three enzyme mediated cases of 1st order Ogden, 3rd order polynomial, 2nd order reduced polynomial and van der Waals model

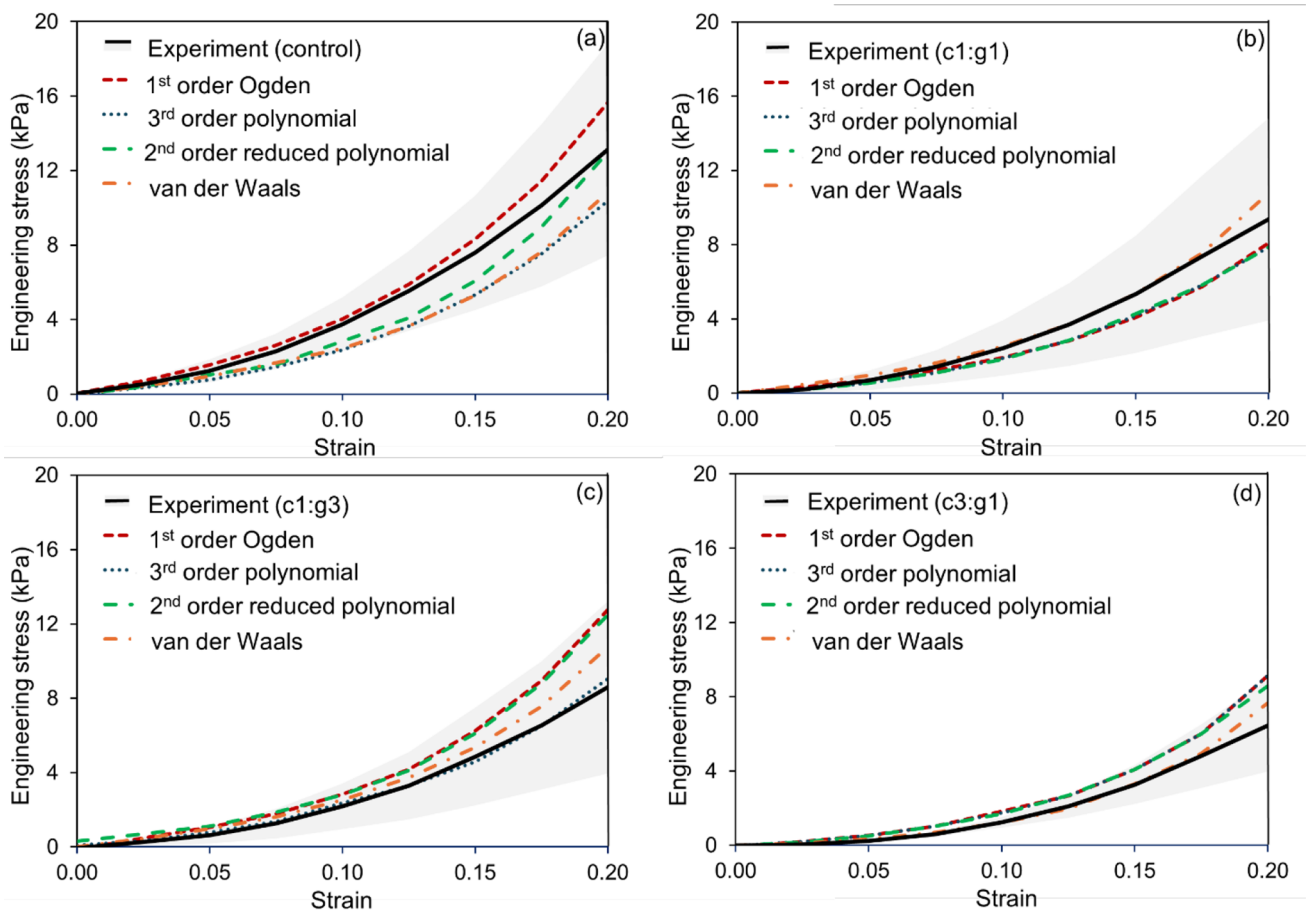

Fig. 4 Stress–strain plots (mean ± *SD*) of native (control) **a** and degraded cartilages—c1:g1 **b,** c1:g3 **c** and c3:g1 **d** based on experiments with fitted hyperelastic material models up to a bulk strain of 20%. The black solid line represents mean engineering stress with upper and lower bounds in gray shaded region (±*SD*). (c: collagenase, g: gelatinase)

models exhibit a moderate level of deviation, except for c1:g3 (Fig. 4c), where the 3rd order polynomial model fitted very well. It is apparent that the van der Waals model fits well with the degraded cartilage (Figs. 4b, c). Figure 5 shows the mean goodness of fit with the hyperelastic models of healthy and degraded groups. Evidently, all the models fit well to the experimental data, the lowest R^2 value of 96.76% for the 1st order Ogden and the highest R^2 values were achieved by the 2nd order reduced polynomial and van der Waals models (99.99%).

Experimental stress–strain plots of the healthy (control) and degraded cartilages along with the FE simulated stress–strain behavior have been shown in Fig. 6. The reaction force was extracted from the loading reference point and then divided by the contact surface area to determine the FE stress. It is evident that while the 1st order Ogden model fitted considerably well with the cartilages in different degraded states (Fig. 4), the corresponding FE simulations (Figs. 6a–d) largely deviate when modeled with the 1st order Ogden model and falls even outside the lower bounds

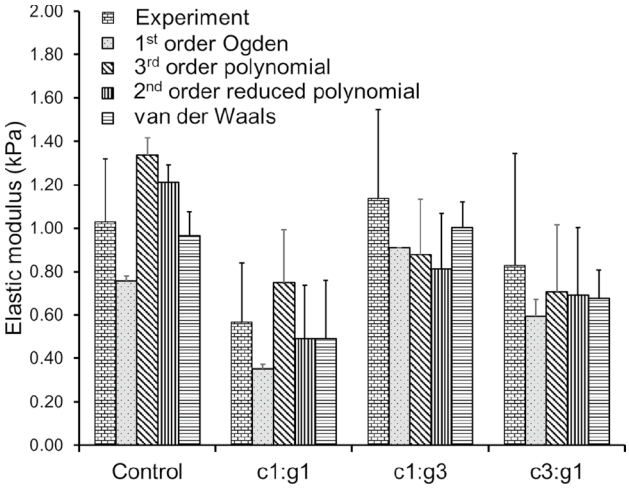

Fig. 7 Comparison of elastic modulus (mean ± *SD*) between the experiments and FE simulations conducted with different hyperelastic material models for healthy (control) and degraded cartilage for c1:g1, c1:g3, and c3:g1 treatment groups. (c: collagenase, g: gelatinase)

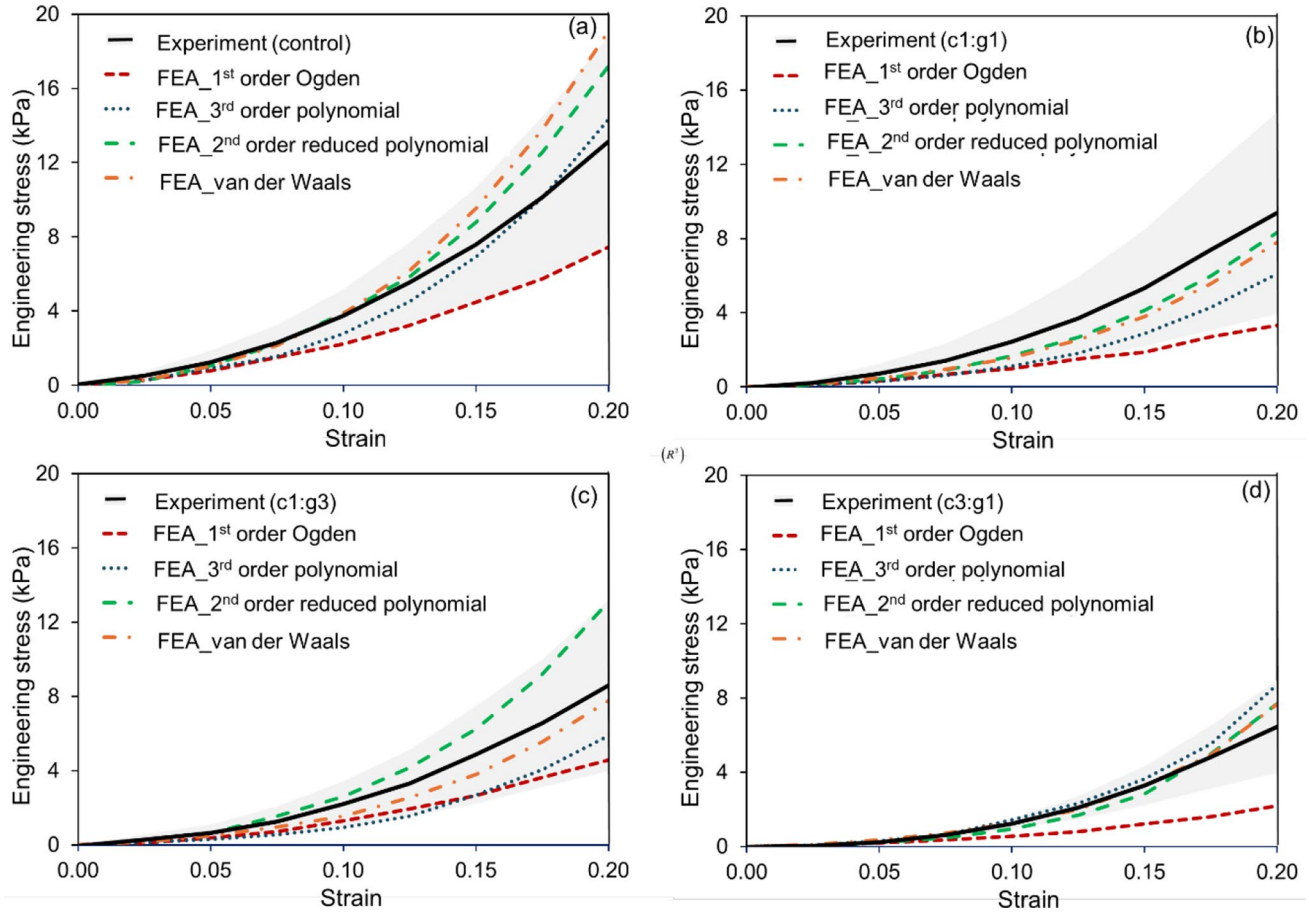

Fig. 6 Stress–strain plots (mean ± *SD*) of the native (control) **a** and degraded cartilages—c1:g1 **b**, c1:g3 **c** and c3:g1 **d** based on experiments and FE simulations using the calibrated hyperelastic material parameters up to a bulk strain of 20%. The black solid line represents mean experimental engineering stress with upper and lower bounds in gray shaded region) (±*SD*). (c: collagenase, g: gelatinase)

of the experimental results. Likewise, the 3rd order polynomial based FE simulated stress–strain curve depicts large variation from the experimental observation except for the cartilage degraded with a c3:g1 concentration ratio (Fig. 6d). However, it is apparent that the FE results with the 2nd order reduced polynomial and van der Waals models exhibit good agreement with our experimental observations, except a moderate deviation of the van der Waals model from the control, and the 2nd order reduced polynomial from the c3:g1 degraded cartilages (Fig. 6d).

Figure 7 shows the comparison of Young's (elastic) modulus of healthy and degraded cartilages between experiments and FEA conducted with the hyperelastic constitutive models. In both cases, the Young's modulus was calculated by linearly fitting the initial portion of the stress–strain curve up to 20% strain with a slow strain-rate without the consideration of instantaneous and equilibrium stages. The differences between the experimental and computational mean values of Young's modulus produced by the 1st order Ogden, 3rd order polynomial, 2nd order reduced polynomial, and van der Waals hyperelastic constitutive models respectively are 26.69%, 29.89%, 17.79%, 6.41% for the control, 38.07%, 31.82%, 13.64%, 13.84% for the c1:g1, 19.83%, 22.70%, 28.45%, 11.78% for the c1:g3, and 28.17%, 14.68%, 16.27%, 18.25% for the c3:g1, samples, respectively. It is apparent that elastic modulus obtained via FEA using van der Waals material model parameters exhibit the closest approximation for both healthy and degraded states.

Figure 8 delineates the FE-simulated stress contours in the cartilage after indentation. With the degradation, the mechanical integrity reduces, which is why a trend of higher stress is observed in the degraded states compared to their control. van der Waals and 2nd order reduced polynomial models yielded better-fitted simulated results among the four selected models. Therefore, the material parameters for the 2nd order reduced polynomial and van der Waals models were discussed herein; the materials data for the 3rd order polynomial and Ogden models are shown in the appendix.

Figure 9 shows the parametric variations between the control and degraded states. Figure 9a depicts that C_{10} decreased from 3.27 to 2.55 kPa for the c1:g1, 6.06 to 3.88 kPa for c1:g3, and 6.54 to 1.30 kPa for c3:g1. It is evident that C_{10}

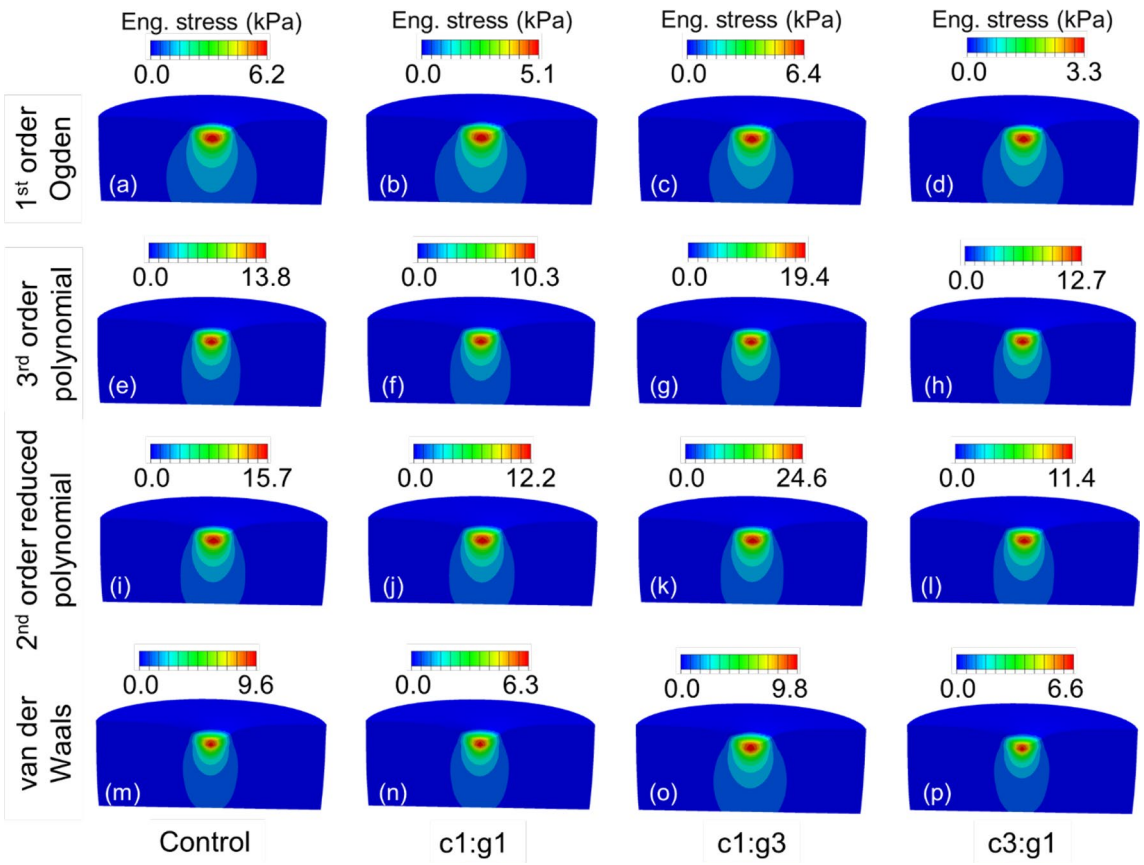

Fig. 8 FE simulated contour plots of the engineering stress of healthy (control) and cartilages treated with the concentration ratio of c1:g1, c1:g3, and c3:g1 using the fitted parameters of the 1st order Ogden **a**–**d**, 3rd order polynomial **e**–**h**, 2nd order reduced polynomial **i**–**l** and van der Waals **m**–**p** models at 20% of applied (compressive) bulk strain. (c: collagenase, g: gelatinase). All the stress contours were shown in the symmetric cross-section on the vertical plane for a clear view of depth-wise stress distributions

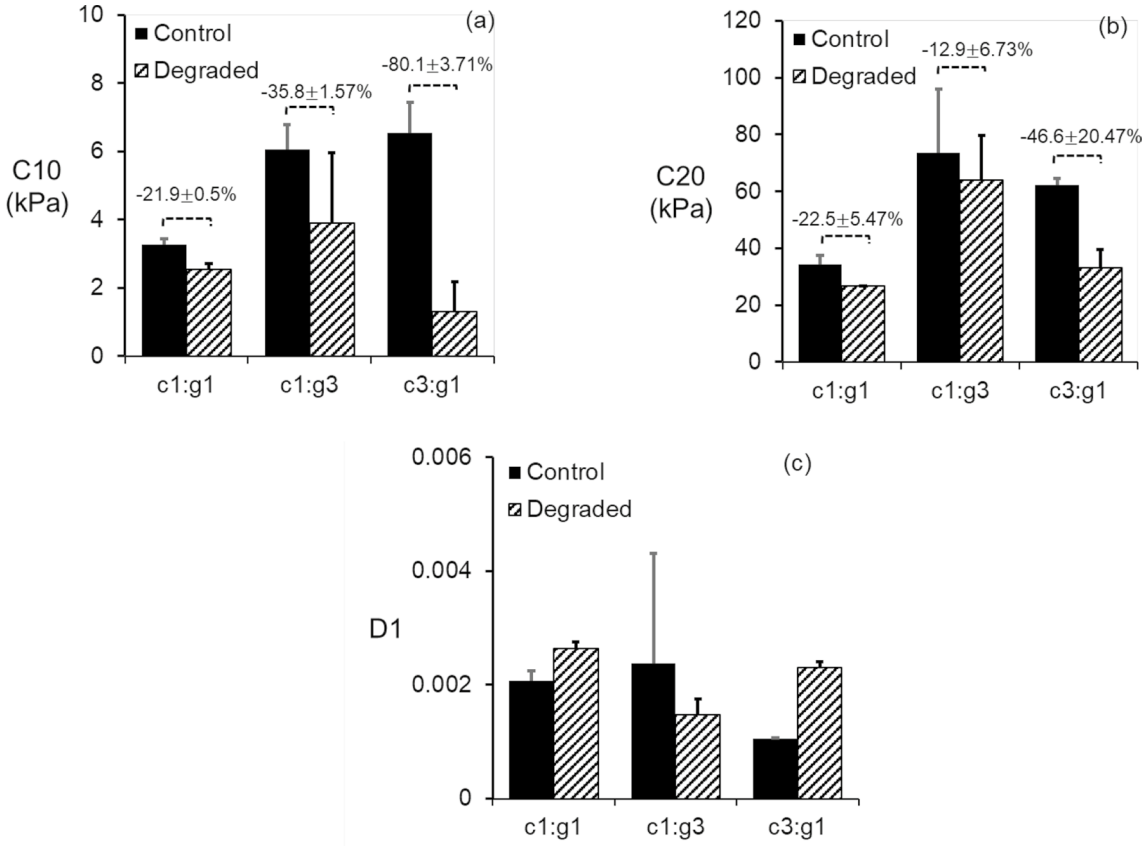

Fig. 9 Variations of the material parameters (mean ± *SD*) of the 2nd order reduced polynomial model using a curve fitting approach. (c: collagenase, g: gelatinase)

decreased significantly in c3:g1 group, which also experimentally exhibited the maximum degradation among the others (Mixon et al. 2021, 2022). The effect of degradation has also been evident in Fig. 9b where C_{20} value shows a maximum of 46.6% reduction in c3:g1 compared with a reduction of 22.5% and 12.9% for c1:g1 and c1:g3, respectively. The compressibility parameter D_1 was found to be nearly zero, while D_2 was determined to be exactly zero.

Figure 10 shows the variations of the material parameters for the van der Waals model. The initial shear modulus (μ) at low strain decreased from 5.91 kPa, 10.79 kPa, 12.48 kPa to 4.22 kPa, 7.82 kPa, 3.84 kPa, respectively, with higher concentrations of collagenase (Fig. 10a), while the locking stretch (λ) remained almost unchanged in response to enzymatic alterations (Fig. 10b). The global interaction parameter a in the polymer chain was almost unaffected by c1:g1 and c3:g1 MMP mixture; however, c1:g3 notably reduced the predicted value of this parameter by 5.5% (Fig. 10c). Despite observing a rise in β values (changing from −0.67 to −1.01 for c1:g1, −0.39 to −1.43 for c1:g3, and − 1.21 to 1.41 for c3g1), a specific sequence pattern could not be identified. The compressibility parameter D_1 exhibited comparatively larger deviation for c1:g3 enzyme concentration.

4 Discussion

Cartilage stiffness varies significantly with type II collagen fibrils packed in the matrix. The fibrils bear the highest tensile stiffness applied on the cartilage, whereas the PG aggregates, occupying the interfibrillar space within the cartilage ECM, may serve as a protective barrier for collagen fibrils against enzymatic denaturation (Mixon et al. 2021; Smith 1999). However, both type II collagen and PGs are essential to OA pathology (Heinegård and Saxne 2011), where aggrecan (PG) loss can be reversed, but not the collagen, and consequently, cartilage cannot be repaired once collagen is largely digested (Karsdal et al. 2008). Collagenases (MMP-1) cleave the collagen triple helix, effectively denaturing the type II collagen network that provides the tissue with its compressive stiffness (Burrage et al. 2006). An increased amount of collagenase concentration is anticipated to enhance fibrillar degradation. Gelatinases (MMP-9) are responsible for cleaving the proteoglycan core protein-aggrecan as well as the fragmented collagen fibrils that turned into gelatin; however, increased MMP-9 concentration alone has minimal impact on aggrecan degeneration (Mixon et al. 2022). When collagenase (a potent enzyme) is present

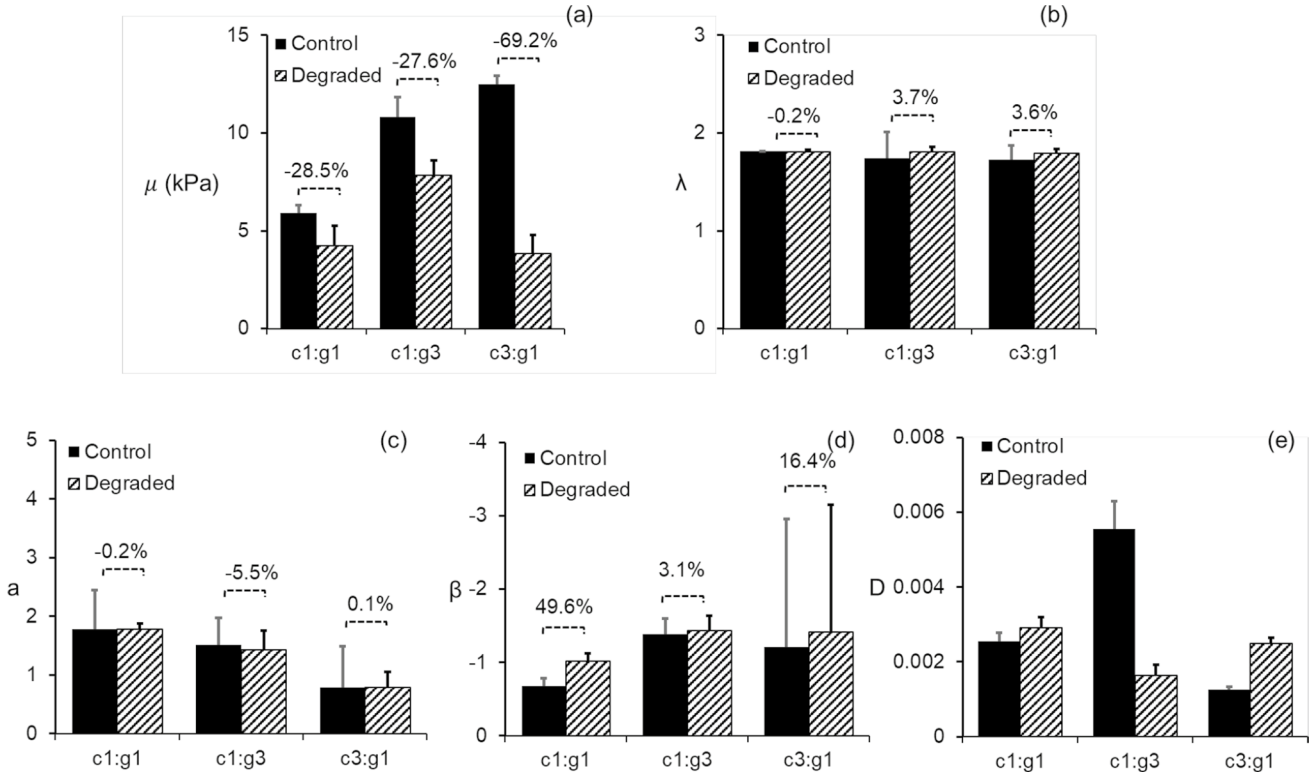

Fig. 10 Variations of the van der Waals model material parameters (mean ± *SD*) using a curve fitting approach. (c: collagenase, g: gelatinase)

alongside gelatinase, compressive stiffness of cartilage is significantly decreased (Burrage et al. 2006). Collagenase denatures type II collagen in the ECM, making it more susceptible to further digestion by gelatinase (MMP-9). Consequently, the peak stress variation between control and treated groups at 20% applied strain is approximately 24% for c1:g1, 29% for c1:g3 and ~ 50% for c3:g1. Our previously published paper qualitatively assessed the zone-wise collagen and PG degradation by histological scoring based on the staining color intensity of safranin O and picrosirius red. Additionally, the computed Pearson correlation coefficient implied strong relationship between the losses of mechanical integrity with the compromised morphological condition of enzyme mediated cartilage (Mixon et al. 2021, 2022).

Deformations of soft tissues involve complex mechanisms that are not fully understood. Phenomenological models have been crafted from macroscopic experimental observations to delineate the nonlinear elastic behavior of materials. In this study, we adopted the phenomenological approach to investigate the nonlinear compressive behavior of cartilage in healthy and degraded states. We determined the hyperelastic material constants of healthy and degraded cartilage using both principal stretch-based (Ogden) and invariant-based (polynomial, reduced polynomial, and van der Waals) phenomenological hyperelastic constitutive models and evaluated the ability of each model to capture different degraded states of cartilages' stress–strain behavior. Isotropic hyperelastic models were previously used to study the mechanical behavior of cartilage at the human hip (Anderson et al. 2008; Henak et al. 2014), human elbow (Willing et al. 2013), human jaw (Koolstra and Van Eijden 2006), porcine knee (Butz et al. 2011), and bovine patella (Brown et al. 2009). However, the choice of an appropriate hyperelastic model relies on various factors, including the associated variables, parameter identification, and the alignment with experimental results. During this study, the models were selected based on the regression analysis of the fitted graphs that yielded coefficient of determination values between 97% and 99% for bulk strains up to 20%. Additionally, models were selected considering their mathematical expressions to facilitate the easy numerical implementation of the model. In order to generate an average predicted graph, every model was simultaneously fitted to all data series for each stress–strain case derived from the indentation test conducted on both healthy and degraded cartilage explants. The current study presents data on the material constants of intact and enzymatically mediated degenerated bovine femoral cartilage derived from the isotropic hyperelastic models. After conducting several calibrations for fitting, we determined the parameter values to be incorporated into FE models.

In this study, first order Ogden, third order polynomial, second order reduced polynomial and van der Waals models

were chosen as they demonstrated superior performance in fitting the experimental data compared to other phenomenological hyperelastic models. Nevertheless, the 1st order Ogden and 3rd order polynomial models exhibited significant deviations between the FE simulated and experimental stress–strain plots, leading us to exclude them from our final consideration. The hyperelastic constants of the 2nd order reduced polynomial model C_{10}, C_{20}, and D_1 and van der Waals model (μ, λ, a, β and D_1) were significantly higher in the control specimens, implying higher cartilage stiffness (Figs. 9 and 10). The lower values of the hyperelastic material constants for the degraded specimens are most likely a consequence of degenerated cartilage associated with the relative abundance of MMP-1 (collagenases) and MMP-9 (gelatinases).

In the second order reduced polynomial model, C_{10} and C_{20} coefficients are associated with the linear and quadratic strain energy density functions, respectively and are dependent on the initial shear modulus and locking stretch. When a material softens with moderate strains, C_{10} represents the initial shear modulus and C_{20} determines the curvature of the strain energy density function, which influences both the nonlinearity and stiffness of a material. In this study, a significant reduction in these two parameters were observed, indicating reduced non-linearity and stiffness that align with enzyme-induced changes in cartilage. The cartilage is incompressible; hence, the compressibility parameters D_1 and D_2 exhibited a very low value or zero.

The load-bearing capabilities of healthy and enzyme-mediated cartilage can be analyzed using the van der Waals hyperelastic model, which is rooted in the understanding of molecular interactions and the mechanical behavior of rubber-like materials (Kilian 1981; Marckmann and Verron 2006). Similar to the experimental data, the initial shear modulus (μ) decreased more in the c3:g1 condition since more load-bearing collagen fibrils were expected to deteriorate by adding a higher concentration of collagenase. Prior experiments showed that the load-bearing ability was significantly reduced for the cartilage degraded with a c3:g1 concentration ratio (Mixon et al. 2021, 2022). Due to a higher concentration of MMP-1 (collaegenases), the fibrils in the superficial zone are digested/degraded more, and thereby reduce its mechanical integrity more than the other two concentration ratios. The unchanged locking stretch (λ) inhibits the significant irreversible deformation at a critical transitional stretch, which can prevent irreversible changes in cartilage after loading. We hypothesized that the global interaction parameter (a) denotes the intensity of molecular interactions with different components in the cartilage matrix, which is primarily determined by the biochemical composition and structural arrangement of its constituents. For example, heightened gelatinase activity for c1:g3 results in considerable degradation of PG aggregates and collagens, which are essential for preserving the cohesive molecular forces within ECM. This decrease aligns with the loss of PG aggregates and collagen loss, which are vital for sustaining cohesive molecular interactions and structural integrity of the ECM. As PG and collagen degradation advances, the reduction in mirrors the declining van der Waals interactions and underscores the disrupted equilibrium of molecular forces in the ECM, ultimately connecting biochemical alterations to mechanical degradation. Although the value of the curve fitted β is in the range of 0 to 1.0, the curve fitting procedure can be used with a user-defined value of β outside the stated range. This parameter is related to the repulsive force, which is a linear mixture parameter combining the invariant I_1 and I_2, where I_1 is more dominant (Seibert and Schoche 2000). D_1 represents the volume changes though the effect is negligible (Holzapfel 2002).

Phenomenological hyperelastic models, rooted in the observations of rubber-like materials undergoing uniform deformation, are structured on the principles of principal stretch. Evaluating the predictive capacity of these models involves comparing their stress–strain or stress-stretch representations with traditional experimental findings (Holzapfel 2002). These models are widely used for modeling biological soft tissues (Kang et al. 2022). Invariant-based phenomenological models are often employed to characterize rubber-like materials, including isotropic materials (Jiang et al. 2022; Melly et al. 2021), focusing on the deformation tensors' principal invariants. However, they cannot explain the molecular-level interaction (Miehe et al. 2004). Although both the second order reduced polynomial and van der Waals models are invariant-based phenomenological models, the 2nd order reduced polynomial explicitly focuses on the first invariant of the deformation tensor. In contrast, the van der Waals model uses a nonlinear least-squares procedure for fitting, which can better capture the nonlinear behavior of hyperelastic materials (ABAQUS 2006), incorporates dependency on both invariants, providing enhanced flexibility and robustness in data fitting, uses parameters from molecular level interaction origin that allow for a more accurate representation of material behavior across different deformation (Lin et al. 2023). Therefore, the van der Waals model has the capability to present cartilage more accurately. The coefficients of the reduced polynomial model can control the shape of the strain energy density function, but this function may not adequately represent the intricate nonlinear behavior exhibited by articular cartilage degraded differentially. Especially when capturing complex phenomena like swelling or compression, it may lack an adequate physical basis to describe the nonlinear behavior of articular cartilage.

Determination of appropriate hyperelastic constitutive model parameters requires comparing model predictions with experimental data. However, due to the substantial

deformations experienced by cartilages and the considerable variation in stress–strain behavior across between (healthy and degraded) state cartilage, it is challenging to establish a single strain energy density function that accurately captures the stress–strain relationship from any experiment (Kim et al. 2016). Another aspect to examine is the extent to which the suggested model parameters in this study can be applied. Although we achieved strong alignments between the hyperelastic material models and experimental findings, the parameter determination process relied solely on one form of experiment, the compression test. Certain hyperelastic models may prove to be less effective when data from a limited range of test types are available (Bidhendi et al. 2020). The Ogden model exhibited an admirable proficiency in accommodating a broad spectrum of experimental data, but calibration based solely on a single type of experiment, such as compression, as in this study, led to significant prediction errors in terms of stresses during FEA. Additionally, obtaining material coefficients by averaging the model results fitted to individual data sets is not recommended as this approach is prone to yielding erroneous or non-physical outcomes (Robertson and Cook 2014).

While this study has significantly advanced our understanding of cartilage mechanics, a number of limitations are acknowledged herein. Our models assume isotropic and homogeneous properties of cartilage, simplifying the inherent complex, anisotropic, and heterogeneous nature of the actual tissue. This assumption is practical for avoiding complexity in more realistic models or when detailed experimental conditions are impractical. Nonetheless, future works should incorporate anisotropic hyperelastic models and depth-dependent properties to better capture cartilage behavior, as demonstrated by previous researchers (Wilson et al. 2005; Li et al. 2000; Pierce et al. 2013). Spherical indenter was used in this study to produce uniform pressure distribution throughout the thickness of the cartilage, thereby minimizing excessive fluid flow across the radial direction. This approach was chosen to mitigate incompressibility, which tends to increase with higher fluid pressure under fast dynamic loading (Anderson et al. 2008; Ateshian et al. 2007). This effectively enhances the load-bearing capacity of the interstitial fluid, maintaining the validity of the incompressibility assumption during the early stages of loading (Park et al. 2003). However, we recognize that as loading duration increases, fluid exudation may occur slowly. To address the fluid effect, future work could incorporate poroelastic models to capture time-dependent fluid flow and tissue compressibility.

In conclusion, we have considered four best fitted phenomenological hyperelastic constitutive models to computationally (via FEA) investigate cartilage mechanics in healthy and degraded states. There is perhaps no generalized fundamental mathematical form of a hyperelastic model (strain-energy density function) that ensures a reasonable mechanical behavior in every possible situation (Ball and James 2002). Accordingly, it is reasonable to say that the second order reduced polynomial and van der Waals model are reasonably well validated with experimental stress–strain data. However, the van der Waals model is the preferred choice for enhanced precision. Furthermore, this research provides well-fitted material parameter models for conducting further computational analyses. Moreover, this study demonstrates how material parametric value evaluation can provide an insight into the degeneration of articular cartilage.

Supplementary Information The online version contains supplementary material available at https://doi.org/10.1007/s10237-024-01919-2.

Author contributions T.F. conceived the idea, and T.F., A.I., and S.I. designed the study. A.I. and S.I. carried out all investigations. A.I., S.I., M.A., and T.F. conducted the data analysis and interpretation of data. All authors (A.I., S.I., M.A., and T.F.) discussed the results and contributed to the drafting of this manuscript. All authors reviewed and approved the final manuscript.

Data availability No datasets were generated or analyzed during the current study.

Declarations

Conflict of interest The authors declare no competing interests.

References

ABAQUS™ (2006) Hyperelastic material behavior
Anderson AE, Ellis BJ, Maas SA, Peters CL, Weiss JA (2008) Validation of finite element predictions of cartilage contact pressure in the human hip joint. J Biomech Eng. 130(5):051008
Armstrong CG, Mow VC (1982) Variations in the intrinsic mechanical properties of human articular cartilage with age, degeneration, and water content. J Bone Joint Surg Am 64:88–94
Ateshian GA, Mow V, Huiskes R (2005) Friction, lubrication, and wear of articular cartilage and diarthrodial joints. Basic Orthopaedic Biomech Mech-Biol 3:447–494
Ateshian GA, Ellis BJ, Weiss JA (2007) Equivalence between short-time biphasic and incompressible elastic material responses. J Biomech Eng. 129:405–412
Athanasiou K, Agarwal A, Dzida F (1994) Comparative study of the intrinsic mechanical properties of the human acetabular and femoral head cartilage. J Orthop Res 12:340–349
Bae WC, Lewis CW, Levenston ME, Sah RL (2006) Indentation testing of human articular cartilage: effects of probe tip geometry and indentation depth on intra-tissue strain. J Biomech 39:1039–1047
Bae W, Schumacher B, Sah R (2007) Indentation probing of human articular cartilage: effect on chondrocyte viability. Osteoarthr Cartil 15(1):9–18
Ball J, James R (2002) The Scientific Life and Influence of¶ Clifford Ambrose Truesdell III. Arch Ration Mech Anal 161:1–26
Bidhendi AJ, Li H, Geitmann A (2020) Modeling the nonlinear elastic behavior of plant epidermis. Botany 98:49–64
Bingham J et al (2008) In vivo cartilage contact deformation in the healthy human tibiofemoral joint. Rheumatology 47:1622–1627

Brown C, Nguyen T, Moody H, Crawford R, Oloyede A (2009) Assessment of common hyperelastic constitutive equations for describing normal and osteoarthritic articular cartilage. In: Proceedings of the Institution of Mechanical Engineers, Part H: Journal of Engineering in Medicine 223:643–652

Budday S et al (2017) Mechanical characterization of human brain tissue. Acta Biomater 48:319–340

Budday S, Ovaert TC, Holzapfel GA, Steinmann P, Kuhl E (2020) Fifty shades of brain: a review on the mechanical testing and modeling of brain tissue. Arch Comput Methods Eng 27:1187–1230

Burrage PS, Mix KS, Brinckerhoff CE (2006) Matrix metalloproteinases: role in arthritis. Front Biosci 11(529):543

Butz KD, Chan DD, Nauman EA, Neu CP (2011) Stress distributions and material properties determined in articular cartilage from MRI-based finite strains. J Biomech 44:2667–2672

Carter TE et al (2015) In vivo cartilage strain increases following medial meniscal tear and correlates with synovial fluid matrix metalloproteinase activity. J Biomech 48:1461–1468. https://doi.org/10.1016/j.jbiomech.2015.02.030

Changoor A, Fereydoonzad L, Yaroshinsky A, Buschmann MD (2010) Effects of refrigeration and freezing on the electromechanical and biomechanical properties of articular cartilage. J Biomech Eng. 132(6):064502

Chen AC et al (2004) Mechanical Characterization of Native and Tissue-Engineered Cartilage. In: De Ceuninck F, Sabatini M, Pastoureau P (eds) Cartilage and Osteoarthritis: Volume 2: Structure and In Vivo Analysis. Humana Press, Totowa

Coleman JL et al (2013) Diurnal variations in articular cartilage thickness and strain in the human knee. J Biomech 46:541–547

Fernandes JC, Martel-Pelletier J, Lascau-Coman V, Moldovan F, Jovanovic D, Raynauld JP, Pelletier JP (1998) Collagenase-1 and collagenase-3 synthesis in normal and early experimental osteoarthritic canine cartilage: an immunohistochemical study. J Rheumatol 25:1585–1594

Fernández JR, López-Campos JA, Segade A, Vilán J (2018) A genetic algorithm for the characterization of hyperelastic materials. Appl Math Comput 329:239–250

Galloway W, Murphy G, Sandy J, Gavrilovic J, Cawston T, Reynolds J (1983) Purification and characterization of a rabbit bone metalloproteinase that degrades proteoglycan and other connective-tissue components. Biochem J 209:741–752

Gasser TC, Holzapfel GA (2002) A rate-independent elastoplastic constitutive model for biological fiber-reinforced composites at finite strains: continuum basis, algorithmic formulation and finite element implementation. Comput Mech 29:340–360. https://doi.org/10.1007/s00466-002-0347-6

Gavin HP (2019) The Levenberg-Marquardt algorithm for nonlinear least squares curve-fitting problems Department of Civil and Environmental Engineering Duke University August 3

Grenier S, Bhargava MM, Torzilli PA (2014) An in vitro model for the pathological degradation of articular cartilage in osteoarthritis. J Biomech 47:645–652. https://doi.org/10.1016/j.jbiomech.2013.11.050

Heinegård D, Saxne T (2011) The role of the cartilage matrix in osteoarthritis. Nat Rev Rheumatol 7:50

Henak CR, Kapron AL, Anderson AE, Ellis BJ, Maas SA, Weiss JA (2014) Specimen-specific predictions of contact stress under physiological loading in the human hip: validation and sensitivity studies. Biomech Model Mechanobiol 13:387–400

Hernandez PA et al (2022) Sexual dimorphism in the extracellular and pericellular matrix of articular cartilage. Cartilage 13:19476035221121790

Holzapfel GA (2002) Nonlinear solid mechanics: a continuum approach for engineering science. Kluwer Academic Publishers, Dordrecht

Jaramillo H, Gomez L, García JJ (2015) A finite element model of the L4-L5-S1 human spine segment including the heterogeneity and anisotropy of the discs. Acta of bioengineering and biomechanics 17

Jiang M, Dai J, Dong G, Wang Z (2022) A comparative study of invariant-based hyperelastic models for silicone elastomers under biaxial deformation with the virtual fields method. J Mech Behav Biomed Mater 136:105522

Kabir W, Bella C, Choong Di PF, O'Connell CD (2021) Assessment of native human articular cartilage: a biomechanical protocol. Cartilage 13(427S):437S

Kaliske M, Rothert H (1997) On the finite element implementation of rubber-like materials at finite strains. Eng Comput 14:216–232

Kang W, Xu P, Yue Y, Wang L, Fan Y (2022) Difference analysis of phenomenological models with two variable forms for soft tissue quasi-static mechanical characterization. Comput Biol Med 150:106150

Kar S, Smith DW, Gardiner BS, Grodzinsky AJ (2016) Systems based study of the therapeutic potential of small charged molecules for the inhibition of IL-1 mediated cartilage degradation. PLOS ONE 11:e0168047. https://doi.org/10.1371/journal.pone.0168047

Kar S, Smith DW, Gardiner BS, Li Y, Wang Y, Grodzinsky AJ (2016) Modeling IL-1 induced degradation of articular cartilage. Arch Biochem Biophys 594:37–53

Karimi A, Shojaei A, Tehrani P (2017) Mechanical properties of the human spinal cord under the compressive loading. J Chem Neuroanat 86:15–18

Karsdal MA, Madsen SH, Christiansen C, Henriksen K, Fosang AJ, Sondergaard BC (2008) Cartilage degradation is fully reversible in the presence of aggrecanase but not matrix metalloproteinase activity. Arthr Res Ther 10(1):12

Khaniki HB, Ghayesh MH, Chin R, Amabili M (2023) Hyperelastic structures: A review on the mechanics and biomechanics. Int J Non-Linear Mech 148:104275

Kilian H-G (1981) Equation of state of real networks. Polymer 22(209):217

Kilian H-G, Enderle H, Unseld K (1986) The use of the van der Waals model to elucidate universal aspects of structure-property relationships in simply extended dry and swollen rubbers. Colloid Polym Sci 264:866–876

Kim S, Jung C-l, Jung Y, Moon H, Lim H Biomimetic skin-type shear sensor. In: 2016 16th International Conference on Control, Automation and Systems (ICCAS), 2016. IEEE, pp 1331–1332

Kiviranta P, Rieppo J, Korhonen RK, Julkunen P, Töyräs J, Jurvelin JS (2006) Collagen network primarily controls Poisson's ratio of bovine articular cartilage in compression. J Orthop Res 24:690–699

Kleemann R, Krocker D, Cedraro A, Tuischer J, Duda G (2005) Altered cartilage mechanics and histology in knee osteoarthritis: relation to clinical assessment (ICRS Grade). Osteoarthritis Cartil 13:958–963

Klets O, Mononen ME, Tanska P, Nieminen MT, Korhonen RK, Saarakkala S (2016) Comparison of different material models of articular cartilage in 3D computational modeling of the knee: Data from the Osteoarthritis Initiative (OAI) Journal of biomechanics 49:3891–3900

Koolstra J, Van Eijden T (2006) Prediction of volumetric strain in the human temporomandibular joint cartilage during jaw movement. J Anat 209:369–380

Korhonen R, Laasanen M, Töyräs J, Rieppo J, Hirvonen J, Helminen H, Jurvelin J (2002) Comparison of the equilibrium response of articular cartilage in unconfined compression, confined compression and indentation. J Biomech 35:903–909

Lagarias JC, Reeds JA, Wright MH, Wright PE (1998) Convergence properties of the Nelder-Mead simplex method in low dimensions SIAM. J Optim 9(112):1476
Levenberg K (1944) A method for the solution of certain non-linear problems in least squares. Q Appl Math 2(164):168
Li L, Buschmann MD, Shirazi-Adl A (2000) A fibril reinforced nonhomogeneous poroelastic model for articular cartilage: inhomogeneous response in unconfined compression. J Biomech 33:1533–1541
Liggett JA, Chen L-C (1994) Inverse transient analysis in pipe networks. J Hydraul Eng 120(934):955
Lin P-S, Roux Le, de Bretagne O, Grasso M, Brighton J, StLeger-Harris C, Carless O (2023) Comparative analysis of various hyperelastic models and element types for finite element analysis. Designs 7:135
Linus A et al (2024) Site-specific elastic and viscoelastic biomechanical properties of healthy and osteoarthritic human knee joint articular cartilage. J Biomech 169:112135
Lohr MJ, Sugerman GP, Kakaletsis S, Lejeune E, Rausch MK (2022) An introduction to the Ogden model in biomechanics: benefits, implementation tools and limitations. Philos Trans R Soc A 380:20210365
López-Campos JA, Segade A, Casarejos E, Fernández JR, Días GR (2019) Hyperelastic characterization oriented to finite element applications using genetic algorithms. Adv Eng Softw 133:52–59
Lotz M, Loeser RFJB (2012) Effects of aging on articular cartilage homeostasis. Bone 51(241):248
Luersen MA, Le Riche R, Guyon F (2004) A constrained, globalized, and bounded Nelder-Mead method for engineering optimization. Struct Multidiscip Optim 27:43–54
Lyyra T, Kiviranta I, Väätäinen U, Helminen HJ, Jurvelin JS (1999) In vivo characterization of indentation stiffness of articular cartilage in the normal human knee. J Biomed Mater Res 48:482–487
Ma J, Arruda EM (2013) A micromechanical viscoelastic constitutive model for native and engineered anterior cruciate ligaments. In: Holzapfel GA, Kuhl E (eds) Computer Models in Biomechanics: From Nano to Macro. Springer, Cham
Mansouri M, Darijani H (2014) Constitutive modeling of isotropic hyperelastic materials in an exponential framework using a self-contained approach. Int J Solids Struct 51:4316–4326
Marckmann G, Verron E (2006) Comparison of hyperelastic models for rubber-like materials. Rubber Chem Technol 79(835):858
Marquardt DW (1963) An algorithm for least-squares estimation of nonlinear parameters. J Soc Ind Appl Math 11(431):441
Melly SK, Liu L, Liu Y, Leng J (2021) A review on material models for isotropic hyperelasticity International Journal of Mechanical System. Dynamics 1:71–88
Merrild NG et al (2022) Local depletion of proteoglycans mediates cartilage tissue repair in an ex vivo integration model. Acta Biomater 149:179–188. https://doi.org/10.1016/j.actbio.2022.06.032
Miehe C, Göktepe S, Lulei F (2004) A micro-macro approach to rubber-like materials—part I: the non-affine micro-sphere model of rubber elasticity. J Mech Phys Sol 52:2617–2660
Mixon A (2021) A Comprehensive in Vitro Study to Investigate the Mutual Effect of MMPs-1 and 9 on Articular Cartilage Biomechanical Properties. University of Louisiana at Lafayette, Lafayette
Mixon A, Savage A, Bahar-Moni AS, Adouni M, Faisal T (2021) An in vitro investigation to understand the synergistic role of MMPs-1 and 9 on articular cartilage biomechanical properties. Sci Rep 11:14409
Mixon A, Bahar-Moni AS, Faisal TR (2022) Mechanical characterization of articular cartilage degraded combinedly with MMP-1 and MMP-9. J Mech Behav Biomed Mater. https://doi.org/10.1016/j.jmbbm.2022.105131
Moerman KM, Fereidoonnezhad B, McGarry JP (2020) Novel hyperelastic models for large volumetric deformations. Int J Solids Struct 193:474–491
Moldovan F, Pelletier JP, Hambor J, Cloutier JM, Martel-Pelletier J (1997) Collagenase-3 (matrix metalloprotease 13) is preferentially localized in the deep layer of human arthritic cartilage in situ: in vitro mimicking effect by transforming growth factor beta. Arthr Rheum 40:1653–1661. https://doi.org/10.1002/art.1780400915
Mooney M (1940) A theory of large elastic deformation. J Appl Phys 11:582–592
Nissinen MT et al (2021) Functional and structural properties of human patellar articular cartilage in osteoarthritis. J Biomech 126:110634
Ogden RW (1972) Large deformation isotropic elasticity–on the correlation of theory and experiment for incompressible rubberlike solids.In: Proceedings of the Royal Society of London A Mathematical and Physical Sciences 326:565–584
Oloyede A, Broom N (1996) The biomechanics of cartilage load-carriage. Connect Tissue Res 34:119–143
Park S, Krishnan R, Nicoll SB, Ateshian GA (2003) Cartilage interstitial fluid load support in unconfined compression. J Biomech 36:1785–1796
Park S, Hung C, Ateshian G (2004) Mechanical response of bovine articular cartilage under dynamic unconfined compression loading at physiological stress levels. Osteoarthritis Cartil 12(65):73
Patel JM, Wise BC, Bonnevie ED, Mauck RL (2019) A systematic review and guide to mechanical testing for articular cartilage tissue engineering tissue engineering Part C. Methods 25:593–608
Pelliciari M, Tarantino AM (2020) Equilibrium paths for von Mises trusses in finite elasticity. J Elast 138:145–168
Pierce DM, Ricken T, Holzapfel GA (2013) A hyperelastic biphasic fibre-reinforced model of articular cartilage considering distributed collagen fibre orientations: continuum basis, computational aspects and applications. Comput Methods Biomech Biomed Eng 16:1344–1361
Pierce DM, Trobin W, Trattnig S, Bischof H, Holzapfel GA (2009) A phenomenological approach toward patient-specific computational modeling of articular cartilage including collagen fiber tracking. J Biomech Eng. 131(9):091006
Previati G, Gobbi M, Mastinu G (2017) Silicone gels-comparison by derivation of material model parameters. Polym Testing 58:270–279
Richard F, Villars M, Thibaud S (2013) Viscoelastic modeling and quantitative experimental characterization of normal and osteoarthritic human articular cartilage using indentation. J Mech Behav Biomed Mater 24:41–52
Rieppo J et al (2003) Structure-function relationships in enzymatically modified articular cartilage. Cells Tissues Organs 175:121–132
Rivlin RS (1948) Large elastic deformations of isotropic materials IV further developments of the general theory philosophical transactions of the royal society of London series a. Math Phys Sci 241(379):397
Rivlin RS, Saunders D (1951) Large elastic deformations of isotropic materials VII experiments on the deformation of rubber philosophical transactions of the royal society of London series a. Mathematical and Physical Sciences 243(251):288
Robertson D, Cook D (2014) Unrealistic statistics: how average constitutive coefficients can produce non-physical results. J Mech Behav Biomed Mater 40:234–239
Robinson DL, Kersh ME, Walsh NC, Ackland DC, de Steiger RN, Pandy MG (2016) Mechanical properties of normal and osteoarthritic human articular cartilage. J Mech Behav Biomed Mater 61:96–109
Saarakkala S, Laasanen M, Jurvelin J, Törrönen K, Lammi M, Lappalainen R, Töyräs J (2003) Ultrasound indentation of normal and

spontaneously degenerated bovine articular cartilage. Osteoarthritis Cartil 11:697–705
Saarakkala S, Töyräs J, Hirvonen J, Laasanen MS, Lappalainen R, Jurvelin JS (2004) Ultrasonic quantitation of superficial degradation of articular cartilage. Ultrasound Med Biol 30:783–792
Sasson A, Patchornik S, Eliasy R, Robinson D, Haj-Ali R (2012) Hyperelastic mechanical behavior of chitosan hydrogels for nucleus pulposus replacement—experimental testing and constitutive modeling. J Mech Behav Biomed Mater 8:143–153
Seibert D, Schoche N (2000) Direct comparison of some recent rubber elasticity models. Rubber Chem Technol 73(366):384
Setton LA, Elliott DM, Mow VC (1999) Altered mechanics of cartilage with osteoarthritis: human osteoarthritis and an experimental model of joint degeneration. Osteoarthritis Cartil 7(2):14
Shearer T (2015) A new strain energy function for the hyperelastic modelling of ligaments and tendons based on fascicle microstructure. J Biomech 48:290–297
Smith RL (1999) Degradative enzymes in osteoarthritis. Front Biosci 4(D704):D712
Smith GN Jr (2006) The role of collagenolytic matrix metalloproteinases in the loss of articular cartilage in osteoarthritis. Front Biosci 11:95
Steck D, Qu J, Kordmahale SB, Tscharnuter D, Muliana A, Kameoka J (2019) Mechanical responses of Ecoflex silicone rubber: compressible and incompressible behaviours. J Appl Polym Sci 136:47025
Suchocki C (2017) Finite element implementation of slightly compressible and incompressible first invariant-based hyperelasticity: theory, coding, exemplary problems. J Theor Appl Mech. https://doi.org/10.15632/jtam-pl.55.3.787
Sui Y et al (2009) Mechanical injury potentiates proteoglycan catabolism induced by interleukin-6 with soluble interleukin-6 receptor and tumor necrosis factor α in immature bovine and adult human articular cartilage Arthritis & Rheumatism: official. J Am Coll Rheumatol 60:2985–2996
Sutter EG, Widmyer MR, Utturkar GM, Spritzer CE, Garrett WE Jr, DeFrate LE (2015) In vivo measurement of localized tibiofemoral cartilage strains in response to dynamic activity. Am J Sports Med 43:370–376
Szarko M, Muldrew K, Bertram JE (2010) Freeze-thaw treatment effects on the dynamic mechanical properties of articular cartilage. BMC Musculoskelet Disord 11:1–8
Tan WS, Moore AC, Stevens MM (2023) Minimum design requirements for a poroelastic mimic of articular cartilage. J Mech Behav Biomed Mater 137:105528
Tchetverikov I, Lohmander LS, Verzijl N, Huizinga TW, TeKoppele JM, Hanemaaijer R, DeGroot J (2005) MMP protein and activity levels in synovial fluid from patients with joint injury, inflammatory arthritis, and osteoarthritis. Ann Rheum Dis 64:694–698. https://doi.org/10.1136/ard.2004.022434
Töyräs J, Rieppo J, Nieminen M, Helminen H, Jurvelin J (1999) Characterization of enzymatically induced degradation of articular cartilage using high frequency ultrasound. Phys Med Biol 44:2723
Treloar LG (1975) The physics of rubber elasticity. Oxford University Press, Oxford
Wang Q et al (2008) Real-time ultrasonic assessment of progressive proteoglycan depletion in articular cartilage. Ultrasound Med Biol 34:1085–1092
Weizel A et al (2022) Hyperelastic parameter identification of human articular cartilage and substitute materials. J Mech Behav Biomed Mater 133:105292
Willing RT, Lalone EA, Shannon H, Johnson JA, King GJ (2013) Validation of a finite element model of the human elbow for determining cartilage contact mechanics. J Biomech 46:1767–1771
Wilson W, Van Donkelaar C, Van Rietbergen B, Huiskes R (2005) A fibril-reinforced poroviscoelastic swelling model for articular cartilage. J Biomech 38:1195-1204
Woo S-Y, Akeson W, Jemmott G (1976) Measurements of nonhomogeneous, directional mechanical properties of articular cartilage in tension. J Biomech 9:785–791
Xia Y, Moody J, Alhadlaq H, Burton-Wurster N, Lust G (2002) Characteristics of topographical heterogeneity of articular cartilage over the joint surface of a humeral head. Osteoarthritis Cartil 10:370–380
Yeoh OH (1993) Some forms of the strain energy function for rubber. Rubber Chem Technol 66(754):771